Shape of Fair Weather Clouds

Yong Wang and Giovanni Zocchi*

Department of Physics and Astronomy, University of California Los Angeles, Los Angeles, California 90095-1547, USA

(Received 7 August 2009; revised manuscript received 19 November 2009; published 18 March 2010)

We introduce a model which accounts for the shape of cumulus clouds exclusively in terms of thermal plumes or thermals. The plumes are explicitly represented by a simple potential flow generated by singularities (sources and sinks) and are thus laminar, but with their motion create a field which supports the cloud. We compare this model with actual clouds by means of various shape descriptors including the fractal dimension, and find agreement.

DOI: 10.1103/PhysRevLett.104.118502 PACS numbers: 92.60.Nv, 47.27.De, 89.75.Fb

It is well known that cumulus clouds (''fair weather clouds,'' Fig. 1) form under the influence of thermals—convection currents which channel moist air upwards. As the temperature of the air drops with altitude, water vapor condenses into droplets; the cloud is the collection of these droplets. Many effects play a role in the formation and dynamics of clouds, such as the dynamics of droplet growth around seeds, the heat released by condensation, and the structure of the turbulent flow. Some of the questions which are investigated experimentally and through modeling include the distribution of droplet size and its evolution [1–3], the spatial distribution of droplets [4,5], the influence of pollutants [6,7], and, of course, conditions for precipitation [8].

Here we concentrate on only one aspect of the cumulus cloud: its characteristic ''cauliflower'' shape (Fig. 1). We introduce a simple model which is based on known properties of thermal plumes; it disregards many of the effects mentioned above, but still produces the familiar shape. First we summarize the relevant properties of convection plumes, established by Moses *et al.* some 20 years ago [9,10]. A thermal plume produced by a localized heat source has a mushroomlike appearance, the cap rising at constant velocity $v_p \propto \sqrt{P}$ where P is the power input to the heater. The fluid velocity field outside the cap is well described by a potential flow which, in the frame of reference of the rising plume, consists of a source and sink plus uniform flow $-v_p$ (Fig. 2). In particular, the shape of the cap is given by the flow line through the stagnation points of this flow (this line separates the ''inside'' of the cap from the ''outside''). The interaction between plumes is well described by the source-sink pair moving according to the flow generated by the other sources and sinks (thus two sinks attract and two sources repel). When two plumes collide, the final state is one new plume fed by twice the power, rising at a velocity $\sqrt{2}v_p$. Finally, laminar plumes exist as long-lived coherent structures in fully turbulent flows, such as high Rayleigh number convection [11]. Our model of the cumulus cloud consists of a collection of such plumes and water droplets. The familiar shape—which is the only characteristic of the cloud which we address—is a consequence of the flow field produced by the plumes.

In more detail: we imagine a fixed vertical temperature gradient in the atmosphere, and a collection of N_d droplets. If a drop falls below the height y_1, it disappears (''evaporates''). All droplets are the same and, for simplicity, the total number of droplets is kept constant, so when one droplet disappears a new one is created at random in the space $y_1 \leq y \leq y_2$. Droplets are advected by the air flow and fall under the force of gravity; the velocity of a droplet at position $\boldsymbol{x}$ is given by

$$\boldsymbol{v} = \boldsymbol{u}(\boldsymbol{x}) - v_d\hat{\boldsymbol{y}}, \tag{1}$$

where $\boldsymbol{u}(\boldsymbol{x})$ is the flow velocity at the position $\boldsymbol{x}$ and $v_d > 0$ is the fall velocity. The flow is created by a collection of N_p rising plumes; when a plume disappears (dissipates) at $y > y_2$ a new plume is created randomly at $y = y_0 < y_1$. Thus N_p is also fixed, and for simplicity all plumes are the same. The velocity of the ith plume is given by

$$\boldsymbol{v}_i = \boldsymbol{u}_i(\boldsymbol{x}) + v_p\hat{\boldsymbol{y}}, \tag{2}$$

where v_p is the rising velocity of the plume and $\boldsymbol{u}_i$ the flow field without the contribution of the ith plume. The flow field $\boldsymbol{u}(\boldsymbol{x})$ in Eq. (1) is the sum of all the contributions from the instantaneous positions of the plumes. A plume starts as a source-sink pair separated by a distance r_0 (Fig. 2). The flow field $\boldsymbol{u}(\boldsymbol{x})$ created by one source of strength s at position $\boldsymbol{x}_i$ is derived from the potential

FIG. 1. Cumulus cloud photographed by the authors in the sky of Philadelphia.

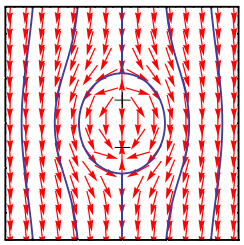

FIG. 2 (color online). In the frame of reference of the ascending plume, the flow outside the plume can be described by a source-sink pair plus a uniform downward flow. The flow line through the stagnation points defines the boundary of the plume.

$$\phi(\boldsymbol{x}) = \frac{s}{|\boldsymbol{x} - \boldsymbol{x}_i|}, \qquad \boldsymbol{u}(\boldsymbol{x}) = -\nabla\phi = s\frac{\boldsymbol{x} - \boldsymbol{x}_i}{|\boldsymbol{x} - \boldsymbol{x}_i|^3}, \quad (3)$$

$s > 0$ for a source, and for the corresponding sink $s \to -s$.

So far the parameters of the model are N_p, s, v_p, v_d, r_0, $h = y_2 - y_1$. To simplify the parameter space, we choose $r_0 = \sqrt{s/v_p}$, which is the distance from the source to the stagnation point (Fig. 2); thus the plume is characterized by a single length scale r_0. A reasonable guess of dimensionless control parameters is then the ratio of the rising velocity of the plume to the falling velocity of the droplets

$$\chi = \frac{v_p}{v_d} \quad (4)$$

and the volume fraction occupied by the plumes

$$\varphi = \frac{N_p r_0^3}{V}, \quad (5)$$

where $V = A \times h$ is the volume of the cloud (A is the area where the plumes are generated). For example, it is intuitive that if χ is small and/or φ is small, droplets fall out of the cloud, whereas if χ is large and $\varphi \sim 1$, the droplets remain in the cloud.

In the simulation we use the cutoff r_0 to handle the collision of plumes: if two sinks approach within r_0, the corresponding two plumes are replaced by a new plume at the "center of mass" position, rising with velocity $\sqrt{2}v_p$. Similarly, when a droplet approaches a sink within r_0, it is moved to a symmetric position in front of the plume. For the sake of convenience, we also ran simulations in 2D; then the velocity potential is $\phi \propto \ln(|\boldsymbol{x} - \boldsymbol{x}_i|)$ and correspondingly $r_0 = s/v_p$, $\varphi = N_p r_0^2/V$ where V is now an area.

Figure 3 shows "snapshots" of the same cloud at different times, obtained from the 2D simulation. The top of the cloud displays the familiar "cauliflower" shape. In real cumulus clouds the average droplet size is in the range 10–50 μm [12,13], which corresponds to fall velocities of 2–100 cm/s. Updraft velocities are in the range 1–10 m/s [14,15], so values of χ between 1 and 10^3 are realistic. Figure 4 shows a snapshot of a cloud obtained with the 3D simulation. The appearance could be improved with a suitable illumination scheme taking into account light scattering inside the cloud [16]; however, this is a separate problem not connected with the hydrodynamic model. Qualitatively, for "large" φ ($\varphi > 0.1$) the top of the cloud becomes more rugged as χ is decreased (we ran simulations for $\chi = 30$ and $\chi = 5$); for "small" φ ($\varphi < 0.1$) the cloud looks already rugged for $\chi = 30$ and as χ is further decreased the top takes on more the appearance of filaments.

For quantitative comparisons, the boundaries of a real cloud and a simulated 2D cloud are extracted from Figs. 1 and 3 (with more droplets), respectively, and shown in the inset of Fig. 5. Commonly used shape descriptors are the

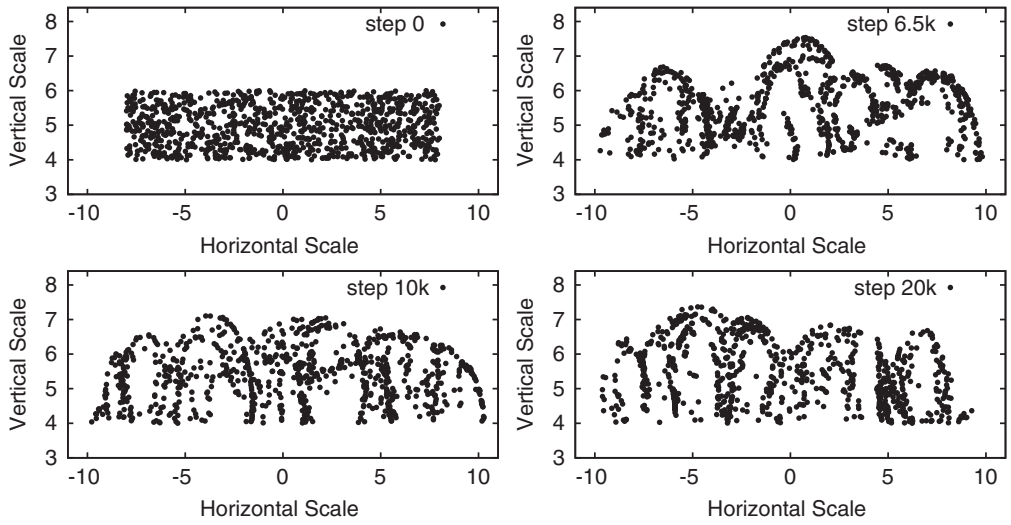

FIG. 3. Four "snapshots" of the distribution of droplets obtained from the same 2D simulation at different times. The initial condition is a uniform, random distribution of droplets. The cloud contains 1000 droplets, and the model parameters were $\varphi = 0.08$, $\chi = 30$, $N_p = 6$.

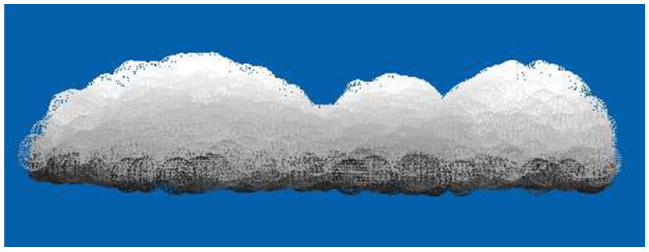

FIG. 4 (color online). Snapshot of the distribution of droplets obtained from the 3D simulation, with $\varphi = 0.1$, $\chi = 10$, $N_p = 9$. The 3D plot was generated using the molecular visualization program VMD [17]: each droplet is represented by a puffy ball.

radius-vector function and curvature function, which we calculate following [18,19]. A reference point O is selected at the center bottom of the cloud. The horizontal line crossing O is chosen as the x axis. The radius-vector function $R(\theta)$ is the distance from the reference point O to the boundary in the direction of θ, and is shown in Fig. 5. Because of the position of O, $0 \leq \theta \leq \pi$. We have normalized the radii R's to [0, 1] in Fig. 5, which amounts to rescaling the size of the clouds. The radius-vector functions of simulated and real clouds are qualitatively similar, reflecting the similarity in global shape of the two clouds. A statistical measure of the behavior of the radius-vector functions is the "roughness coefficient" σ, defined as [18]

$$\sigma = \frac{1}{\Delta\theta}\int_{\theta_m}^{\theta_M} R^2(\theta)d\theta - \left(\frac{1}{\Delta\theta}\int_{\theta_m}^{\theta_M} R(\theta)d\theta\right)^2, \quad (6)$$

where $\Delta\theta = \theta_M - \theta_m$ is the range of the angle θ and $\theta_M = \max(\theta)$, $\theta_m = \min(\theta)$. The difference of roughness coefficients between the simulation and the real cloud (Fig. 5) is $\delta_\sigma \lesssim 5\%$.

An alternative shape descriptor is the curvature κ as a function of arc length s [18]:

$$\kappa(s) = \frac{d\theta(s)}{ds}. \quad (7)$$

Based on the boundary data shown in the inset of Fig. 5, we

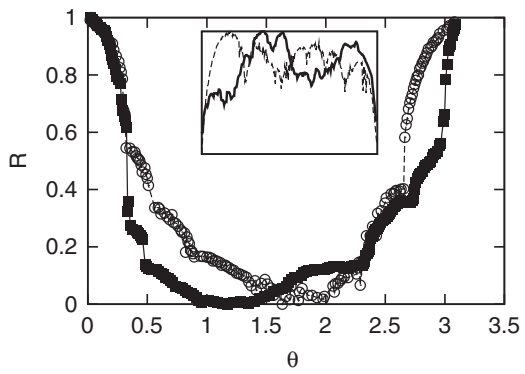

FIG. 5. Radius-vector functions of a real cloud (filled squares) and a simulated cloud (circles) based on the boundaries (the inset) of the real cloud (thick, solid) from Fig. 1 and a simulated cloud (thin, dashed) from Fig. 3 (but with $N_d = 10\,000$ droplets).

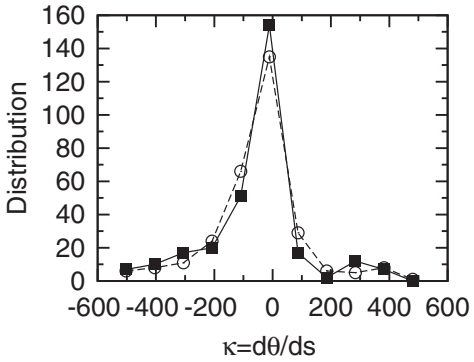

FIG. 6. The distribution of the curvature of the real cloud (filled squares) of Fig. 1 and the simulated cloud (circles) of Fig. 5. Both distributions are negative skewed and non-Gaussian.

calculated the curvature functions. If we compare the "bending energies"

$$E = \frac{1}{L}\int_0^L \kappa(s)^2 ds \quad (8)$$

we find a difference of $\delta_E \approx 13\%$. The (unnormalized) distribution of the curvature κ is plotted in Fig. 6. While the similarity between the model and the real cloud is obvious, more interesting are their negative skewness. The distributions are left skewed, which reflects the fact that the boundary of clouds consists more of caps (⌢⌢⌢) than cups (⌣⌣⌣). In addition, the distributions are not Gaussian. Large κ's in both the simulated cloud and real cloud are more frequent than in the Gaussian distribution.

It has been remarked that clouds have fractal shapes in a range of scales [20–22], with fractal dimensions ranging from 1.164 [21] to 1.35 [22]. Figure 7 shows the estimated fractal dimensions of the real cloud (Fig. 1) and the simulated cloud (Fig. 3 with $N_d = 10\,000$) using the box-counting algorithm [23], $D = \log[n(r)]/\log(1/r)$, where

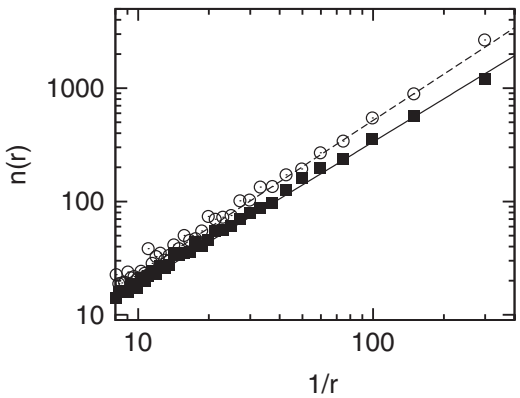

FIG. 7. Graph of the box-counting algorithm applied to the boundaries of the real cloud (filled squares) in Fig. 1 and the same simulated cloud (circles) as in Fig. 5. $n(r)$ is the number of boxes of size r needed to cover the cloud boundary. The slopes give the corresponding fractal dimensions: $D_r = 1.26 \pm 0.01$ (real) and $D_s = 1.36 \pm 0.01$ (simulated).

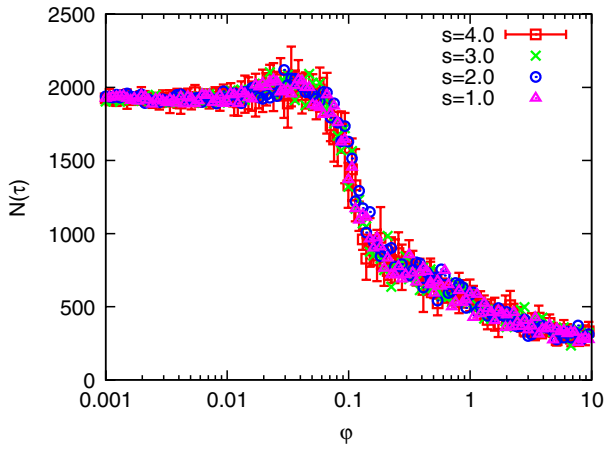

FIG. 8 (color online). The number of droplets $N(\tau)$ which "evaporate" (fall below the line $y = y_1$) in the time $\tau = h/v_d$. The volume fraction of plumes φ is varied keeping $\chi = 30$ and $N_p = 6$ constant (thus τ varies with varying φ). The data collapse for different values of s indicates that φ, χ, and N_p specify the dynamical state of the system. The data are from the 2D simulation. A transition is apparent for $\varphi \sim 0.1$.

$n(r)$ is the number of boxes of size r needed to cover the cloud boundary. The fractal dimensions obtained from Fig. 7 are $D_r = 1.26 \pm 0.01$ and $D_s = 1.36 \pm 0.01$, for real and simulated cloud, respectively.

For a given volume V of the cloud, the model is specified by the 4 parameters N_p, s, v_p, v_d. The time scale, $\tau = h/v_d$, represents the lifetime of the cloud in the absence of plumes. However, in the regime where the cloud is supported by plumes, three out of these four parameters are sufficient to determine the dynamical state of the cloud. Choosing φ, χ, N_p as control parameters, we can then explore the phase diagram of the model. For example, Fig. 8 shows the number of droplets which "evaporate" (fall below the line $y = y_1$) in the time τ, $N(\tau)$, plotted vs φ at constant χ and N_p. The figure shows that graphs obtained for different values of s collapse onto a single curve (i.e., φ, χ, N_p are a complete set of control parameters). We also see a transition in the behavior of the system for $\varphi \approx 0.1$.

In conclusion, we introduce a model which accounts for the shape of cumulus clouds in terms of thermal plumes. The physical effects which pertain to the formation and dynamics of clouds—thermal convection, adiabatic expansion, condensation and evaporation, and so on—are of course well known, and indeed realistic clouds are obtained by integrating the corresponding set of differential equations with appropriate effective terms to link the thermodynamics and fluid motion [16,24]. Alternative formulations in terms of coupled map lattices are similarly useful in discussing the "phase diagram" of clouds [25]. At the other extreme, one can also produce realistic looking clouds by constructing heuristic random density fields with the measured statistical properties of clouds [26]. The present approach starts not with the equations of fluid motion, but at a "mesoscopic" level with the coherent structures which form in the flow. This is reminiscent of quasiparticles in other condensed matter systems, a concept which so far has been of limited utility in the theoretical representation of hydrodynamic turbulence. However, it appears that for this system, the shape of the cloud is determined by these coherent structures.

*zocchi@physics.ucla.edu

[1] H. R. Pruppacher and J. D. Klett, *Microphysics of Clouds and Precipitation* (Springer, New York, 1996).
[2] T. Nakajima and M. D. King, J. Atmos. Sci. **47**, 1878 (1990).
[3] R. McGraw and Y. Liu, Phys. Rev. Lett. **90**, 018501 (2003).
[4] A. Marshak *et al.*, J. Atmos. Sci. **62**, 551 (2005).
[5] M. Wilkinson, B. Mehlig, and V. Bezuglyy, Phys. Rev. Lett. **97**, 048501 (2006).
[6] F.-M. Breon, D. Tanre, and S. Generoso, Science **295**, 834 (2002).
[7] M. O. Andreae and D. Rosenfeld *et al.*, Science **303**, 1337 (2004).
[8] A. Arakawa and W. H. Schubert, J. Atmos. Sci. **31**, 674 (1974).
[9] E. Moses *et al.*, Europhys. Lett. **14**, 55 (1991).
[10] E. Moses, G. Zocchi, and A. Libchaberii, J. Fluid Mech. **251**, 581 (1993).
[11] G. Zocchi, E. Moses, and A. Libchaber, Physica (Amsterdam) **166A**, 387 (1990).
[12] J. Warner, J. Atmos. Sci. **26**, 1272 (1969).
[13] J. W. Telford *et al.*, Q. J. R. Meteorol. Soc. **119**, 631 (1993).
[14] J. Warner, J. Atmos. Sci. **27**, 682 (1970).
[15] P. Kollias *et al.*, J. Atmos. Sci. **58**, 1750 (2001).
[16] M. J. Harris *et al.*, in *Proceedings of the ACM SIGGRAPH/EUROGRAPHICS Conference on Graphics Hardware* (Eurographics Association, San Diego, CA, 2003), pp. 92–101.
[17] W. Humphrey, A. Dalke, and K. Schulten, J. Mol. Graphics **14**, 33 (1996).
[18] V. V. Kindratenko, J. Math. Imaging Vis. **18**, 225 (2003).
[19] S. Loncaric, Pattern Recog. **31**, 983 (1998).
[20] B. B. Mandelbrot, *The Fractal Geometry of Nature* (W. H. Freeman, New York, 1983).
[21] S. Lovejoy, in *Proceedings of the 20th Conference on Radar Meteorology* (American Meteorological Society, Boston, 1981).
[22] S. Lovejoy, Science **216**, 185 (1982).
[23] J. Theiler, J. Opt. Soc. Am. A **7**, 1055 (1990).
[24] R. Miyazaki *et al.*, in *Proceedings of the 9th Pacific Conference on Computer Graphics and Applications* (IEEE Computer Society, Los Alamitos, 2001), p. 0363.
[25] T. Yanagita and K. Kaneko, Phys. Rev. Lett. **78**, 4297 (1997).
[26] G. Y. Gardner, SIGGRAPH Comput. Graph. **19**, 297 (1985).